

# Learning to Detect Entanglement

Bingjie Wang<sup>\*†</sup>

September 13, 2017

## Abstract

This paper introduces the forest algorithm, an algorithm that can detect entanglement through the use of decision trees generated by machine learning. Tests against similar tomography-based detection algorithms using experimental data and numerical simulations indicate that, once trained, the proposed algorithm outperforms previous approaches. The results identify entanglement detection as another area of quantum information where machine learning can play a helpful role.

## 1 Introduction

Machine learning is a powerful tool that is finding far-reaching interdisciplinary connections. The intersection of quantum information and machine learning includes quantum versions of machine learning algorithms and the use of machine learning to analyse quantum systems [1, 2]. This paper explores the latter and identifies entanglement detection as an area where machine learning can improve current practice.

Entanglement is a defining feature of quantum information. Detection algorithms are typically based on either quantum state tomography or entanglement witnesses [3, 4]. Witnesses can reveal entanglement in a single measurement, but only for a small portion of states. This drawback makes witnesses difficult to use without prior information about the underlying state. Tomography does not require prior information, but the number of measurements quickly becomes unreasonable.

Nonetheless, Laskowski *et al* devised an algorithm based on the geometric criterion [5, 6, 7] that may perform tomography, but only in extreme cases. The improvement over quantum state tomography, as measured by the expected number of measurements required, is exponential in the number of qubits. Central is the exploitation of fundamental statistical properties, namely, correlation complimentarity [8]. The paper refers to this method as the tree algorithm.

This paper proposes the forest algorithm for entanglement detection. The algorithm combines ideas from the tree algorithm and quantum state tomography, namely the Bayesian methods from Granade, Combe, and Cory [9]. Instead of using Bayes theorem to obtain the required probability distributions, the forest algorithm models them directly through a random forest. Machine learning allows the forest algorithm to exploit the statistical patterns in more sophisticated ways. Empirical evidence indicates that the forest algorithm outperforms the tree algorithm.

Section 2 presents the previous work in entanglement detection and tomography. The main idea of this paper, the forest algorithm, is presented and discussed in Section 3. Section 4 demonstrates the performance improvement from the forest algorithm on both experimental and simulated data for two to five qubit states.

## 2 Previous Work

In this paper, pure states are denoted by  $|\varphi\rangle$  and mixed states by  $\rho$ . While this paper focuses on pure states, a “state” can be either pure or mixed unless otherwise stated. Likewise, the qubit regime is assumed, but the analysis can be adapted to other systems.

A separable pure state admits the factorization:  $|\varphi\rangle = |\phi_1\rangle \otimes |\phi_2\rangle \otimes \cdots \otimes |\phi_N\rangle$ , where  $N$  is the number of qubits. Similarly, separable mixed states can be expressed in the following form:

$$\rho = \sum_i p_i \rho_1 \otimes \rho_2 \otimes \cdots \otimes \rho_N$$

where  $\sum_i p_i = 1$ . Non-separable states are entangled.

The term measurement is used in two senses. Measuring a set of positive operator value measures (POVMs) returns a single probabilistic result. Given a state,  $\rho$ , and an observable,  $B$ , measurement denotes finding the expectation of the corresponding POVMs on  $\rho$ . The result is denoted by  $\langle B \rangle = \text{tr}(\rho^\dagger B) = \text{tr}(\rho B)$ , with the state implicit. This assumes the experimental setup contains a source producing copies of  $\rho$  to allow accurate estimates of the expectation. The “size” of an observable refers to the relative *magnitude* of  $\langle B \rangle$ .

Quantum state tomography was originally posed as an algebraic inverse problem: given a set of measure-

<sup>\*</sup>Electronic address: bwang297 [at] bloomberg [dot] net

<sup>†</sup>Bloomberg L.P., New York, United States and University of Cambridge, Cambridge, United Kingdom. The views presented in this paper are solely the views of author, and do not necessarily represent those of Bloomberg, L.P. or any of its affiliates.

ment results on POVMs, infer the state  $\rho$ . It is helpful to specify some standard parameterizations. Consider the space of linear operators acting on a  $D$ -dimensional Hilbert space. This space has an orthonormal basis,  $B$ , for the inner product  $\langle B_1, B_2 \rangle = \text{tr}(B_1^\dagger B_2)$ . Under this basis, the quantum state  $\rho$  can be represented as:

$$\rho = \frac{1}{D} \cdot \text{id} + \sum_{i=1}^{D^2-1} x_i B_i \quad (1)$$

where  $\text{id}$  is the identity operator and  $B_0$  is taken to be  $\text{id}/\sqrt{D}$ . Under this setup, tomography can be seen as estimating the parameters  $x_i = \langle B_i \rangle$ . For the qubit regime, the Pauli matrices — in a broad sense to include tensor products of the usual single qubit Pauli matrices,  $\sigma_0 = \text{id}, \sigma_1 = \sigma_x, \sigma_2 = \sigma_y, \sigma_3 = \sigma_z$  — can be used as the basis. For non-qubit regimes, Gell-Mann matrices may be used.

To simply notation,  $B$  will henceforth refer to the Pauli basis. It is convenient to designate  $\bar{B}$  as the tensor products of Pauli matrices minus the identity matrix.

According to the geometric criterion [5], a quantum state,  $\rho$ , is entangled if:

$$\sum_{a_1=1}^3 \sum_{a_2=1}^3 \cdots \sum_{a_N=1}^3 \langle \sigma_{a_1} \otimes \sigma_{a_2} \otimes \cdots \otimes \sigma_{a_N} \rangle^2 = \sum_{B_i \in \bar{B}} \langle B_i \rangle^2 > 1 \quad (2)$$

Once the (partial) sum exceeds one,  $\rho$  can be declared entangled without additional measurements. An optimal strategy would be to measure the largest observables first. However, since measurement results are not known in advance, they must be estimated. Tomography is a possible choice for the estimation process.

## 2.1 Tree Algorithm

Instead of estimating the parameters,  $x_i$ , fundamental statistical properties can be used as heuristics. Correlation complementarity [8] states, for a mutually anti-commuting set of observables  $S$ :

$$\sum_{B \in S} \langle B \rangle^2 \leq 1$$

If an observable,  $B^*$ , is large, then measurements of observables that anti-commute with  $B^*$  are not likely to significantly contribute towards proving entanglement. The tree algorithm analytically constructs a decision tree which tells the user what to measure next if the current observable is small or large. The purpose of the tree is to conduct an organized search of  $\bar{B}$  while avoiding observables which are constrained by correlation complementarity.

Given  $B^*$ , the tree construction is as follows:

1. Compute  $S = \{B \in \bar{B} \mid B \text{ and } B^* \text{ commute}\}$ .

2. Compute the maximal mutually commuting subsets of  $S, Q$ .
3. Sort each  $Q_i$  lexicographically using any ordering on  $\bar{B}$  that places  $B^*$  first.
4. Sort  $Q$  lexicographically. Let the sorted sets be  $\bar{Q}$  and  $\bar{Q}_{i,j}$  denotes the  $j$ -th element in the  $i$ -th subset of  $\bar{Q}$ .
5. If  $\bar{Q}_{i,j}$  is large (i.e.,  $\langle \bar{Q}_{i,j} \rangle^2 > 0.25$ ), measure  $\bar{Q}_{i,j+1}$ . Otherwise, let  $k$  be the first point where  $\bar{Q}_{i,k} \neq \bar{Q}_{i+1,k}$ , measure  $\bar{Q}_{i+1,k}$ .

$B^*$ , as Laskowski *et al* suggest in [7], can be obtained by finding the Bloch vectors of each qubit (at a cost of three measurements per qubit).

If the tree does not prescribe a measurement target, compute the priority for the unmeasured observables. An observable's priority is the sum of the squared expectations over all measured observables that anti-commute with it. Measurements are continued in ascending order of priority.

While the algorithm is deemed to be “optimized”, there are possible areas for improvements. For example, the suggested method for finding  $B^*$  does not contribute to proving entanglement. In addition, while the tree algorithm’s performance is insensitive to the “largeness” threshold  $\langle \bar{Q}_{i,j} \rangle^2 > 0.25$ , there is little reason to treat observables marginally above or below the threshold differently. Both issues are addressed by the forest algorithm.

## 2.2 Bayesian Tomography

One way to estimate the parameters is Bayesian tomography, devised by Granade, Combes, and Cory [9]. Suppose the measurement results  $M$  are obtained from the POVMs  $\{E_1, E_2, \dots, E_k\}$ , then the Born rule gives the likelihood:

$$\text{pr}(M|\rho) = \text{tr}[E_1 \rho]^{n_1} \text{tr}[E_2 \rho]^{n_2} \cdots \text{tr}[E_k \rho]^{n_k}$$

where  $n_k$  is the number of times  $E_k$  is observed in  $M$ . Equipped with the likelihood, Bayes theorem yields:

$$\text{pr}(\rho|M) d\rho \propto \text{pr}(M|\rho) \cdot \text{pr}(\rho) d\rho \quad (3)$$

which is a distribution that can be used to construct the Bayesian mean estimate:  $\hat{\rho} = \int \rho \cdot \text{pr}(\rho|M) d\rho$ . The term  $\text{pr}(\rho) d\rho$  is referred to as the prior and  $\text{pr}(\rho|M)$  is referred to as the posterior. Initially, the following uninformative prior is used:

$$\rho \sim U(|0 \cdots 0\rangle \langle 0 \cdots 0|) U^\dagger \quad (4)$$

where  $|0 \cdots 0\rangle$  denotes  $|0\rangle^{\otimes N}$  and  $U$  is drawn according to the Haar measure on  $N$ -qubit unitaries. After making measurements and computing the posterior by Eq.

3, the posterior then becomes the prior for further inference. Further details on priors, such as priors for mixed states, are available in [9], as well as the discussion in Section 3.3.

This procedure can be used as part of a *simple* entanglement detection scheme. Given a Pauli matrix,  $B$ , its POVMs are  $(\text{id} \pm B)/2$ . The measurement encoded by  $H$  corresponds to a binary experiment with outcome probabilities of  $(1 \pm \langle B \rangle)/2$ . The experiment is repeated until  $\langle B \rangle$  can be estimated with sufficient confidence. After obtaining  $\langle B \rangle$ , Bayes' theorem is applied with the measurement results to obtain a new  $\hat{\rho}$ . Through  $\hat{\rho}$ , the required estimates are obtained.

The above scheme is simple in the sense that it works at the observable level. Strategies can use individual measurement results and switch back and forth between measurement settings. It is difficult to compare these schemes within in this paper's context and are not in scope. Such schemes are discussed by Blume-Kohout, Yin, and van Enk in [10].

### 3 Forest Algorithm

In the simple Bayesian tomography algorithm, a subset of measurement results are used to infer the measurement results of the remaining observables in  $\overline{B}$ . This is done through  $\rho$  as a latent variable. Instead, the forest algorithm attempts to do the inference directly. Start by modelling one parameter given all others. Let  $\mathbf{x}$  be the vector of  $\langle B_i \rangle^2$ 's in  $\overline{B}$ , the goal is to estimate:

$$\overline{f}_i(\mathbf{x}) = \overline{f}_i(x_i, \mathbf{x}_{-i}) = \text{pr}(\langle B_i \rangle^2 = x_i | \mathbf{x}_{-i}) \quad (5)$$

where  $\mathbf{x}_{-i}$  is  $\mathbf{x}$ , but with the  $i$ -th component removed.

Now, suppose the  $\overline{f}_i$ 's are available. Conditioning on the known results and marginalizing out the remaining unknowns yields the distributions of each unknown  $\langle B_i \rangle$ . However, it is unrealistic to expect a tractible expression for Eq. 5, let alone integrate it. The task is simplified by incorporating the details of the entanglement detection problem.

Since only the largest observable is of interest, the following proxy of equation 5 is used:

$$\hat{f}_i(x_i, \mathbf{x}_{-i}) = \mathbb{I} \left[ (x_i = \max_j x_j) \text{ given } \mathbf{x}_{-i} \right] \quad (6)$$

where  $\mathbb{I}(\cdot)$  is the indicator function.

Section 3.1 presents how to sample points from  $\hat{f}_i$  and fit an appropriate functional form through machine learning. Once the  $\hat{f}_i$ 's are learned, the forest can be used indefinitely. Section 3.2 describes the detection portion: scores are computed for each unmeasured observable based on the known results. The measurement with the highest score is made and the scores are updated. Finally, Section 3.3 discusses the motivations behind this particular choice of machine learning setup.

### 3.1 Training

In (supervised) machine learning, the input can be described by a vector  $\mathbf{x}$  and the output by  $y$ . Given a training set of  $(\mathbf{x}, y)$  samples, the machine learning algorithm learns the input-output relationship,  $f(\mathbf{x})$ , by fitting  $f$  to the training set. A more comprehensive and detailed treatment is presented in [11].

Fitting Eq. 6 can be cast as a machine learning problem with  $x_i$  as the output,  $y$ , and  $\mathbf{x}_{-i}$  as the input,  $\mathbf{x}$ . This is the widely-studied classification problem;  $\hat{f}_i = 1$  is commonly referred to as the "positive" class and  $\hat{f}_i = 0$  as the negative class. The input-output examples can be obtained by sampling the uninformative prior in Eq. 4. As a reminder, there are  $|\overline{B}|$  such  $\hat{f}_i$ 's, each must be learned in a separate instance of the machine learning problem.

In the forest algorithm,  $f$  is a random forest, which is a collection of decision trees. A decision tree partitions the input space into regions,  $r_1, r_2, \dots, r_k$ , with associated output values,  $y_1, y_2, \dots, y_k$ . The output of a tree is:

$$f(\mathbf{x}) = \sum_{i=1}^k y_i \cdot \mathbb{I}(\mathbf{x} \in r_i)$$

The  $f$  associated with a random forest is the average of its constituent decision trees.

The algorithm to determine  $\{r_i\}$  and  $\{y_i\}$  was independently developed by Quinlan-Ross [12] and Breiman *et al* [13]. An extensive discussion is also provided in [11]. A sketch is provided as follows. Initially, the tree has one region containing the entire input space. The samples falling into a region is viewed as a data source producing 1s and 0s and a region's entropy can be computed. High entropy regions are split by a decision rule,  $x_j \leq \theta$ , chosen to minimize the entropy of the two resulting regions. Splitting continues until all regions have low entropy. The output for each region is determined by the region's majority class. For example, if 10 training set examples fall in the region, of which 7 are positive and 3 are negative, the tree outputs positive.

A number of best practices regarding to random forests should be followed.

- The training set is made to have an equal number of positive and negative examples. With naïve sampling, negative examples dominate the training set and a tree representing  $f(\mathbf{x}) = 0$  will have negligible entropy.

Rejection sampling is used to reject negative (or positive) examples until the required number of positive (or negative) examples are obtained. However, this is expensive. The cost is kept relatively tractible by generating training sets for all learning instances together, applying Clifford unitaries to create positive samples from positive samples in other instances, and repeating positive samples.

- For averaging to be effective, the constituent trees must be decorrelated. Bootstrap aggregation [14] is used to achieve this: constituent trees are trained on a training set constructed by sampling the original training set with replacement. In addition, when selecting the decision rule,  $x_j \leq \theta$ , only a random subset of  $j$ s are considered.
- Decision trees are to be pruned. This not only reduces overfitting, but also makes the detection task in Section 3.2 easier. For a given decision tree, the examples not used for training (out-of-bag examples) can be used as a testing set. Trees are progressively pruned, stopping when the out-of-bag error would be worsened.

## 3.2 Detecting

Let  $\mathbf{x}^*$  be a vector containing the known measurement results. The task of the detection phase is to produce a recommendation for which observable to measure next, given  $\mathbf{x}^*$ . This is done by assigning a score to each possible choice. A natural choice for the score is:

$$\text{pr}(x_i = \max_j x_j | \mathbf{x}^*) = \mathbb{E} \left[ \hat{f}(\mathbf{x}) | \mathbf{x}^* \right]$$

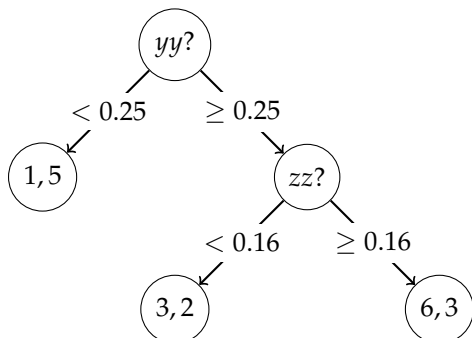
where  $\mathbb{E}[\cdot]$  is the expectation; recall, the expectation of an event's indicator is the probability of the event.

To compute the score, consider a single tree. Let  $p(r)$  and  $n(r)$  respectively be the number of positive and negative training samples falling in the region  $r$ , then an approximation for the above expectation is:

$$\frac{1}{\sum_{r_i \cap \mathbf{x}^* \neq \emptyset} p(r_i) + n(r_i)} \left[ \sum_{r_i \cap \mathbf{x}^* \neq \emptyset} 1 \cdot p(r_i) + 0 \cdot n(r_i) \right]$$

The notation  $r_i \cap \mathbf{x}^* \neq \emptyset$  indicates that the region is still “reachable”, that is, there is no measurement result that contradicts any decision rule  $r_i$ .

A detailed example of the scoring mechanics is given here. Consider the following “toy” tree attempting to predict if  $\langle \sigma_x \otimes \sigma_x \rangle$  is the largest, represented as a graph. Here, the decision rule  $|\langle \sigma_a \otimes \sigma_b \rangle| < \theta$  is represented by a node  $ab?$  and an edge  $< \theta$  and similarly for the  $\geq$  case. A terminal node contains  $p(r)$  and  $n(r)$  respectively.



Let the known measurement results be  $\langle \sigma_y \otimes \sigma_y \rangle^2 = 0.36$  and  $\langle \sigma_z \otimes \sigma_z \rangle^2 = 0.01$ . The score would be:  $3/(3+2) = 0.6$  as only the centre node is reachable.

The score of the forest is the *median* of the tree scores. In addition, if too many regions are unreachable, then the score is discarded. In addition to stabilizing performance and limiting overfitting from outlier trees, these measures “soften” the impact at the boundary of the decision rules, a known issue with the tree algorithm. Furthermore, the presentation so far has not used additional information, whereas the tree algorithm requires a large measurement result to be known in advance.

## 3.3 Concentration of Measure

The relationships between the  $\langle B_i \rangle^2$ s are well captured by random forests. This is a consequence of the special properties of the uninformative prior used.

It is well known that a continuous measure that is invariant under unitary transformations is a uniform measure. For a group,  $(G, \oplus)$ , the Haar measure,  $\mu$ , is the measure such that, for any  $S \subseteq G$  and  $g \in G$ ,  $\mu(S) = \mu(\{g \oplus s | s \in S\}) = \mu(\{s \oplus g | s \in S\})$ . Sampling unitary matrices from its Haar measure is unitary invariant by definition. As expected, the prior represents a uniform distribution. However, Lévy's Lemma [15] states: if  $f$  has Lipschitz constant  $\eta$  (that is,  $|f(\mathbf{x}) - f(\mathbf{y})| \leq \eta \|\mathbf{x} - \mathbf{y}\|$ ) and  $X$  is sampled according to the uniform measure on the  $k$ -dimensional sphere, then:

$$\text{pr}(|f(X) - m_f| > \sqrt{\varepsilon}) \leq \exp \left[ -(k-1)\varepsilon / (2\pi^2 \eta^2) \right]$$

where  $m_f$  is the median of  $f$  under the same measure.

Consider the expectation as a function. First, convert  $|\varphi\rangle$  into the real vector,  $\varphi = [\varphi^r, \varphi^i]^t$ , where  $\varphi^r$  and  $\varphi^i$  are the vectors containing the real and imaginary parts of  $|\varphi\rangle$  respectively. Then, for a Pauli matrix,  $B$ :

$$\langle B \rangle = \text{tr} [|\varphi\rangle \langle \varphi| \cdot B] = \sum_{jk} (\varphi_j^r - i\varphi_j^i)(\varphi_k^r + i\varphi_k^i) B_{kj} = f(\varphi)$$

Lévy's Lemma can be applied to  $f$ , as  $\varphi$  is now uniformly distributed on the  $2^{N+1}$  dimensional sphere. The partial derivatives of  $f$  are:

$$\begin{aligned} \frac{\partial f}{\partial \varphi_m^r} &= 2\varphi_m^r B_{mm} + \sum_{j \neq m} \varphi_j^* B_{mj} + \sum_{k \neq m} \varphi_k B_{km} \\ \frac{\partial f}{\partial \varphi_m^i} &= 2\varphi_m^i B_{mm} + i \sum_{j \neq m} \varphi_j^* B_{mj} - i \sum_{k \neq m} \varphi_k B_{km} \end{aligned}$$

Now, bound  $(\nabla f)^\dagger (\nabla f)$ :

$$\begin{aligned} &(\nabla f)^\dagger (\nabla f) \\ &= \sum_m \left( \frac{\partial f}{\partial \varphi_m^r} \right)^* \left( \frac{\partial f}{\partial \varphi_m^r} \right) + \left( \frac{\partial f}{\partial \varphi_m^i} \right)^* \left( \frac{\partial f}{\partial \varphi_m^i} \right) \\ &= 2 \sum_m |\varphi_m|^2 \cdot |B_{mm}|^2 + 2 \sum_{jk} \varphi_j^* \varphi_k \left( \sum_m B_{km} B_{mj} \right) \end{aligned}$$

The sum has been simplified by noting that the Pauli matrices are Hermitian. The first term is bounded by  $2\sum_m |\varphi_m|^2 = 2$  and the second is  $\text{tr}[|\varphi\rangle\langle\varphi| \cdot B^2] = 1$ , as Pauli matrices square to identity. This bound is an appropriate value for  $\eta^2$ . Finally, Applying Lévy's Lemma shows that  $\langle B \rangle^2 < \varepsilon$  with high probability, that is, with probability  $1 - o(1)$ .

On the other hand, using similar arguments, Hayden, Leung, and Winter show in [16] that sampling from the uniform measure results in states that resemble the maximally entangled state with high probability.

Combining the two results explains the following observation: for a given state, most observables are small, but a subset of observables are very large (in order to violate the geometric criterion). For different states, different observables are large. This large/small behaviour is easily captured by the decision rules, making random forests a good machine learning algorithm for this task.

## 4 Experiments

For two qubits, the forest and tree algorithms can be compared directly using the experimental results available from [7]. The forest algorithm's performance is also showcased for a small selection of common experimental states. Finally, a systematic comparison between the forest, tree, and simple tomography algorithms is run using simulated data.

For the most part, only pure states are considered. Take a pure state corrupted by white noise with probability  $p$ :

$$\rho = (1 - p)|\varphi\rangle\langle\varphi| + p \cdot \text{id}$$

During detection, the relevant results would be scaled by  $1 - p$ . The order of measurements would be unchanged compared to the original pure state.

The forests were generated using the scikit-learn package [17]. Each forest contains 64 generated trees, where 64 was chosen by minimizing out-of-bag error (see Section 3.1). The simple tomography algorithm described in Section 2.2 was implemented using the QInfer package [18]. 300 shots was considered sufficient for establishing an appropriate confidence interval on the expectation.

Throughout,  $a_1 a_2 \cdots a_N$  is used as a shorthand for  $\sigma_{a_1} \otimes \sigma_{a_2} \otimes \cdots \otimes \sigma_{a_N}$ .

### 4.1 Showcase

The states from Laskowski *et al*'s experiment are used here for a direct comparison. The experimentally obtained measurement results are available from [7]. The results for non-maximally entangled states are recalled and presented in Figure 1. The two algorithms have comparable performance, with a slight edge to the forest algorithm.

(a)	<i>x</i>	<i>y</i>	<i>z</i>
<i>x</i>	<b>0.845</b>	-0.068	-0.200
<i>y</i>	-0.211	0.128	<b>-0.911</b>
<i>z</i>	-0.077	-0.849	0.053
(b)	<i>x</i>	<i>y</i>	<i>z</i>
<i>x</i>	<b>0.649</b>	0.031	-0.019
<i>y</i>	-0.130	-0.618	<b>-0.160</b>
<i>z</i>	-0.062	-0.014	<b>0.984</b>
(c)	<i>x</i>	<i>y</i>	<i>z</i>
<i>x</i>	<b>-0.801</b>	0.037	0.357
<i>y</i>	-0.117	<b>0.069</b>	<b>-0.968</b>
<i>z</i>	-0.071	0.842	0.007
(d)	<i>x</i>	<i>y</i>	<i>z</i>
<i>x</i>	<b>0.806</b>	-0.008	0.052
<i>y</i>	-0.144	<b>-0.810</b>	0.134
<i>z</i>	-0.006	0.044	-0.994
(e)	<i>x</i>	<i>y</i>	<i>z</i>
<i>x</i>	<b>0.069</b>	<b>-0.859</b>	0.156
<i>y</i>	<b>-0.976</b>	0.118	-0.029
<i>z</i>	0.016	0.108	<b>0.815</b>
(f)	<i>x</i>	<i>y</i>	<i>z</i>
<i>x</i>	<b>-0.022</b>	<b>0.028</b>	<b>0.128</b>
<i>y</i>	<b>-0.033</b>	<b>-0.042</b>	<b>0.039</b>
<i>z</i>	<b>-0.027</b>	<b>-0.012</b>	<b>0.970</b>

Figure 1: The performance of the forest and tree algorithms on a selected set of states in [7]. The first system appears on columns and the second on rows. **Bold** indicates a measurement made by the forest algorithm. *Italics* indicates a measurement made by the tree algorithm. In case (f), if the preliminary measurements are included, the tree algorithm performs tomography.

The three qubit Dicke states are:

$$|D_1^3\rangle = \frac{1}{\sqrt{3}} [ |001\rangle + |010\rangle + |100\rangle ]$$

$$|D_2^3\rangle = \frac{1}{\sqrt{3}} [ |011\rangle + |101\rangle + |110\rangle ]$$

The forest algorithm detects entanglement in  $|D_1^3\rangle$  and  $|D_2^3\rangle$  after measuring  $xxx$ ,  $xyz$ , and  $zzz$ . The tree algorithm performs better, using  $xxx$  and  $xzz$  only. For the four qubit Dicke state with two excitations:

$$|D_2^4\rangle = \frac{1}{\sqrt{6}} [ |0011\rangle + |0101\rangle + |0110\rangle + |1001\rangle + |1010\rangle + |1100\rangle ]$$

The forest detects entanglement after  $xzxz$ ,  $zxxx$ , and  $zxzx$ . The tree does so after  $xxxx$ ,  $zyzx$ , and  $yxxy$ .

Gdańsk states extend Dicke states:

$$|G(\alpha)\rangle = \cos(\alpha)|D_2^3\rangle + \sin(\alpha)|D_1^3\rangle$$

For  $\alpha \in [0, \pi/2]$ , uniform sampling estimates the average number of measurements the forest algorithm requires for such states is 4.7. The execution trace for  $|G(37\pi/64)\rangle$  is showcased below.

$i$	$B_i$	$\langle B_i \rangle$	$B_i, B_{i-1}$ anti-commute?
1	$xxx$	-0.471	—
2	$xzz$	0.314	false
3	$yxy$	-0.157	true
4	$zxy$	0.000	true
5	$xyz$	0.000	true
6	$xyx$	0.000	true
7	$xzx$	-0.588	true
8	$zxx$	-0.588	false

Evidently, the trained forest recognizes correlation complimentarity, avoiding anti-commuting measurements when it has found a large expectation.

## 4.2 Accessible States

For a robust empirical comparison, the performance should be compared across sufficiently large sample of states. To generate this sample, our experiment constructs a source to draw test states from. Then, the detection algorithms are run on states sampled from this source and the number of measurements made before proving entanglement is compared.

One choice for the source would be the uninformative prior. However, this gives an unfair advantage to the forest algorithm, as it is trained on such a source. In this setting, the forest algorithm outperforms the tree algorithm by 3% for two qubits and 20% for five qubits. In addition, the number of states which are experimentally accessible is countable, whereas the sample space is uncountable. As the number of qubits increases, the uniform source becomes increasingly dissimilar to the source of states that can be practically accessible. Thus, such a comparison may be inappropriate.

Instead, an  $N$ -qubit state is generated as follows. First, generate the number of gates to apply,  $n$ , by drawing from a Poisson distribution. Then construct:

$$|\varphi\rangle = G_1 G_2 \cdots G_n (|0\rangle^{\otimes N})$$

where  $G_i$  applies a gate from the universal set:

$$\left\{ \frac{1}{\sqrt{2}} \begin{bmatrix} 1 & 1 \\ 1 & -1 \end{bmatrix}, \begin{bmatrix} 1 & 0 \\ 0 & e^{i\pi/4} \end{bmatrix}, \text{CNOT} \right\}$$

on one or two uniformly randomly qubits and identity on the remaining qubits.  $24 \cdot N \cdot (N - 1)$  was used as the mean of the Poisson distributions. 48 degrees of freedom provides sufficient diversity for two qubits and the quadratic scaling is based on the number of ways to place a two qubit gate in a  $N$  qubit system.

Figure 2 presents the results across 2000 states sampled using the above distribution, but with an addition rejection sampling step to force the condition  $\langle \sigma_x \otimes \sigma_x \cdots \sigma_x \rangle^2 \geq 0.25$ . This is to accomodate the tree algorithm's need for a starting point. In this setting, the simple tomography algorithm performs poorly. However, this is unsurprising as the algorithm is designed for measurements on POVMs, as opposed to on observables. The performance of the forest and tree algorithms are nearly identical for two qubits, but the forest algorithm has a growing edge as the number of qubits increases. Due to this growing edge, it is conjectured that the forest algorithm is an improvement in general.

## 5 Conclusion

This paper presents how machine learning, through the forest algorithm, can be used in entanglement detection. Empirical evidence shows that the forest algorithm is an improvement, for two to five qubits, over the existing tree algorithm. It is conjectured that this is the case in general. The success of the forest algorithm identifies an area of quantum information processing where machine learning can play a role.

The forest algorithm's direct modeling of the parameter distributions presents a novel and possibly interesting view on quantum state tomography. Although the algorithm is specialized for entanglement detection using the geometric criterion, it is interesting to consider other applications. An immediate application is its use as heuristic for quantum state tomography, in the same manner as it used in this paper. Since the largest observable yields the most information about the state, making measurements recommended by the forest allows the experimenter to quickly narrow down the possible range of states. To convert from the observable regime to the POVM regime, the sample mean can be used, but it is unknown how well such a method would work. It is also possible that the approach taken in this paper can be specialized in another way for other tasks in the analysis of quantum systems.

In short, developments in machine learning provide powerful statistical methods that can be added to the arsenal for the analysis of quantum systems. This paper presents one possible application and encourages the exploration of such applications.

**Acknowledgements.** BW thanks Debbie Leung for help on the concentration of measure and general support throughout the writing of the manuscript. A large part of this work was completed while BW was a student at Cambridge and BW is grateful for the supervision received from Stephen Brierley and Anuj Dawar.

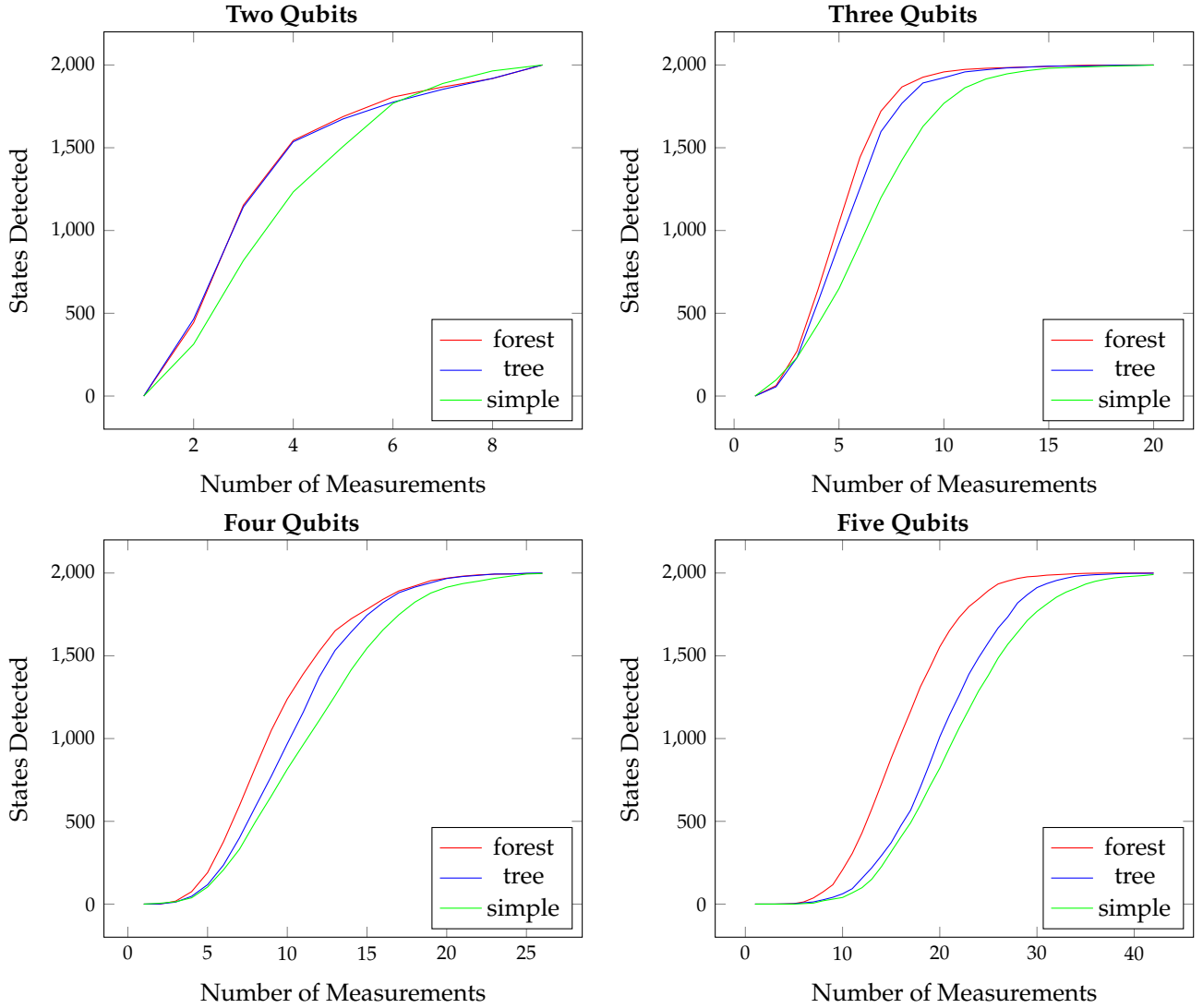


Figure 2: The performance of the tree and forest algorithms on sample of 2000 experimentally accessible states.

## References

- [1] M. Schuld, I. Sinayskiy, and F. Petruccione. An introduction to quantum machine learning. *Contemporary Physics*, 56(2):172–185, 2015.
- [2] J. Biamonte, P. Wittek, N. Pancotti, P. Rebentrost, N. Wiebe, and S. Lloyd. Quantum machine learning. *arXiv preprint*. arXiv:1611.09347, 2016.
- [3] R. Horodecki, P. Horodecki, M. Horodecki, and K. Horodecki. Quantum entanglement. *Reviews of Modern Physics*, 81(2):865, 2009.
- [4] O. Ghne and G. Tth. Entanglement detection. *Physics Reports*, 474(1):1–75, 2009.
- [5] P. Badziag, . Brukner, W. Laskowski, T. Paterek, and M. ukowski. Experimentally friendly geometrical criteria for entanglement. *Physical Review Letters*, 100:140403, 2008.
- [6] W. Laskowski, D. Richart, C. Schwemmer, T. Paterek, and H. Weinfurter. Experimental schmidt decomposition and state independent entanglement detection. *Physical Review Letters*, 108(24):240501, 2012.
- [7] W. Laskowski, C. Schwemmer, D. Richart, L. Knips, T. Paterek, and H. Weinfurter. Optimized state-independent entanglement detection based on a geometrical threshold criterion. *Physical Review A*, 88(2):022327, 2013.
- [8] P. Kurzyski, T. Paterek, R. Ramanathan, W. Laskowski, and D. Kaszlikowski. Correlation complementarity yields Bell monogamy relations. *Physical Review Letters*, 106:180402, 2011.

- [9] C. Granade, J. Combes, and D. Cory. Practical bayesian tomography. *New Journal of Physics*, 18(3):033024, 2016.
- [10] R. Blume-Kohout, J. O. S. Yin, and S. J. van Enk. Entanglement verification with finite data. *Physical Review Letters*, 105(17):170501, 2010.
- [11] G. James, D. Witten, T. Hastie, and R. Tibshirani. *An Introduction to Statistical Learning*. Springer, 2013.
- [12] J. Quinlan Ross. Induction of decision trees. *Machine Learning*, 1(1):81–106, 1986.
- [13] L. Breiman, J. Friedman, C. Stone, and R. Olshen. *Classification and regression trees*. CRC press, 1984.
- [14] L. Breiman. Bagging predictors. *Machine Learning*, 24(2):123–140, 1996.
- [15] M. Ledoux. *The Concentration of Measure Phenomenon*. Number 89. American Mathematical Society, 2005.
- [16] P. Hayden, D. Leung, and A. Winter. Aspects of generic entanglement. *Communications in Mathematical Physics*, 265(1):95–117, 2006.
- [17] F. Pedregosa, G. Varoquaux, A. Gramfort, V. Michel, B. Thirion, O. Grisel, M. Blondel, P. Prettenhofer, R. Weiss, V. Dubourg, J. Vanderplas, A. Passos, D. Cournapeau, M. Brucher, M. Perrot, and E. Duchesnay. Scikit-learn: Machine learning in Python. *Journal of Machine Learning Research*, 12:2825–2830, 2011.
- [18] C. Granade, C. Ferrie, I. Hincks, S. Casagrande, T. Alexander, J. Gross, M. Kononenko, and Y. Sanders. QInfer: Statistical inference software for quantum applications. *Quantum*, 1:5, 2017.